Ensemble statistics of bedload transport. Part 1: Grain motion at near-threshold conditions

Sophie Bodek[1], Dong Wang[2], Mark D. Shattuck[3], Corey S. O'Hern[2,4,5], Nicholas T. Ouellette[1]

[1]Department of Civil and Environmental Engineering, Stanford University, Stanford, CA 94305
[2]Department of Mechanical Engineering, Yale University, New Haven, CT 06520
[3]Benjamin Levich Institute and Physics Department, The City College of New York, New York, NY 10031
[4]Department of Applied Physics, Yale University, New Haven, CT 06520
[5]Department of Physics, Yale University, New Haven, CT 06520

Key Points:

- We use grain tracks from laboratory experiments to characterize ensemble statistics of bedload motion across a range of fluid shear stresses
- We use a hidden Markov model to segment grain trajectories into periods of motion and rest
- We validate previously proposed ensemble distributions for grain velocity, flight distance, and travel time

Corresponding author: Sophie Bodek, `sbodek@stanford.edu`

Abstract

In recent decades, there has been increasing effort toward modeling bedload transport using statistical ensembles for grain velocities, flight distance, and travel times. The forms of these probability distributions are integral to estimating sediment flux, with implications for predicting sediment transport in both natural and engineered systems. In this study, we analyze a high-resolution dataset of grain motions collected from laboratory flume experiments to extract these distributions. We recorded videos of a sand bed exposed to increasing fluid shear ranging from below the nominal threshold stress for grain motion to well above ($\tau_*/\tau_{*cr} = 0.78$–1.53). We extracted trajectories of a population of sand grains and used a hidden Markov model to predict the states of motion and rest from observed grain velocities. We characterize probability distributions for the activity, velocity, acceleration, flight distance, and travel times of moving grains and largely find agreement with previous studies. Streamwise velocities are well fit by an exponential distribution, accelerations display a Laplace distribution, flight travel times also show an exponential distribution, while flight distances are described by a Weibull distribution. We note, however, that these distributions described our data more poorly for bedload motion at and below the expected threshold of motion, especially for flight travel times, suggesting that bedload dynamics differ in this most intermittent regime. These experimental results provide a reference dataset for validating numerical simulations or analytical solutions for stochastic sediment transport models, especially for flow conditions at and below the nominal critical Shields stress.

Plain Language Summary

The periodic flights and rests of sediment grains moving along a riverbed, known as bedload transport, can be described as a stochastic—or random—process. The number of grains that are dislodged, the distance they travel, and the speed of these flights can all be represented as random variables. By characterizing these grain-motion metrics via probability distributions, we can better predict sediment transport in natural and engineered systems. Experimental data is instrumental to validate proposed statistical distributions for parameters of interest, including grain activity, velocity, acceleration, flight distance, and travel time. In this study, we collect high-resolution images of sediment motion at a variety of flow conditions, ranging from slow flows where grain movement is highly intermittent to rapid flows where grains readily move downstream. From these images, we can identify tracks of individual sediment grains and distinguish periods of motion from rest. We measure probability distributions that largely agree with previous studies, especially for flow conditions when grains are readily moving as bedload. However, these distributions fit more poorly for very intermittent grain motion, emphasizing the need for additional study of bedload behavior below the nominal onset of bulk motion.

1 Introduction

Bedload transport is a fundamental physical process that shapes fluvial, coastal, and aeolian landscapes with broad implications for water quality, aquatic life, and infrastructure safety (García, 2013). The movement of sediment as bedload consists of repeated sequences of grains entrained by an overlying shear flow, then rolling, hopping, or sliding a variable distance along the sediment bed (from a few particle diameters to multiple flight-collision sequences) before returning to rest (Dey & Ali, 2019). The initiation of motion and downstream transport of sediment as bedload is highly stochastic due to the variable nature of the grain sizes and the configuration of the sediment bed itself (Kirchner et al., 1990), fluctuations within the shearing turbulent flow (Einstein & El-Samni, 1949), inherent randomness in the entrainment and disentrainment of grains (Cheng & Chiew, 1998), and the range of particle velocities and displacements that occur during the grain flights (Roseberry et al., 2012; S. L. Fathel et al., 2015). By treating the collective behavior of sediment grains as a statistical ensemble (i.e., a large number of independent but nominally identical systems initially introduced by Gibbs (1902)), we can then characterize quantities of interest by probability distributions with physical interpretability—an approach initially pioneered by Einstein (1950, 1937, 1942) and Kalinske (1947) and recently touted by Furbish (2025). Many studies in the intervening years have sought to describe the mechanics of bedload transport as stochastic processes (Weeks et al., 1996; Niño & García, 1998; Ancey et al., 2006; Ancey, 2010; Ancey & Heyman, 2014; Furbish & Schmeeckle, 2013; Furbish, Haff, et al., 2012; Foufoula-Georgiou & Stark, 2010; Fan et al., 2014, 2016; Bradley et al., 2010; Pelosi et al., 2014; Schumer et al., 2009).

However, it is only recently that developments in high-speed imaging and automated particle tracking techniques have permitted large-scale data collection contributing to clear descriptions of individual and collective particle motions (M. X. Liu et al., 2019; Rebai et al., 2024; Shim & Duan, 2017, 2019; Salevan et al., 2017; Campagnol et al., 2013; Lajeunesse et al., 2010; Roseberry et al., 2012; S. L. Fathel et al., 2015) and advances in numerics for coupled fluid-particle dynamics have provided additional validation for experimental observations (González et al., 2017; Schmeeckle & Nelson, 2003; Schmeeckle, 2014; Durán et al., 2012; Escauriaza et al., 2023; Yadav et al., 2026). Stochastic models for bedload transport are more computationally efficient compared to direct numerical simulations of fluid and particle flows; however, stochastic models require input probability distribution parameters for grain velocities, flight distances, and corresponding travel times, along with grain rest times (Schumer et al., 2009; Fan et al., 2014, 2016). Thus, statistical descriptions of grain motion and rest variables are instrumental to improving these stochastic approaches, including probabilistic parameterizations of sediment flux.

Sediment flux is frequently parameterized in a stochastic advection-diffusion formulation in two distinct approaches. First is the "flux form" or "activity form," which is defined for quasi-steady conditions with an advective part consisting of the product of a mean particle velocity $\langle u_g \rangle$ and a particle activity γ (that is, the volume of particles in motion per unit streambed area) (Kalinske, 1947) and a diffusive part involving a particle diffusivity with a magnitude that depends on the variance of the particle velocities (Furbish, Haff, et al., 2012; Furbish, Roseberry, & Schmeeckle, 2012; Ancey & Heyman, 2014; Heyman et al., 2014; Bohorquez & Ancey, 2015). In this formulation, the statistical description of grain accelerations constrains the conditions of quasi-steady, equilibrium sediment transport and quantifies the magnitudes of forces associated with grain entrainment and disentrainment (Furbish & Schmeeckle, 2013; Furbish, Roseberry, & Schmeeckle, 2012). The second approach is frequently called the "entrainment form," with an advective part consisting of the product of the particle entrainment rate E and a mean hop distance $\langle L_x \rangle$ (Einstein, 1950) and a diffusive part that involves the variance of the hop distances (Furbish, Haff, et al., 2012). In this formulation, parameters for flight distance and travel time along with flight rest times have implications for the diffusion of bedload tracer particles (Nikora et al., 2002; Martin et al., 2012; Ganti et al., 2010). For example, the presence of narrow tails in the probability distributions of flight distance, travel time, and rest time suggest that the particle diffusion regime is normal across the local and global scales (Weeks et al., 1996). Alternatively, a heavy-tailed power-law behavior for flight distance may imply superdiffusive behavior (Ganti et al., 2010; Schumer et al., 2009). Better insight into the problem of bedload transport can thus be gained from the separate modeling of grain velocity, activity, and the joint probabilities of flight distance and travel time, as well as how these grain motion parameters vary as a function of bed stress intensity or other flow characteristics.

Existing studies of the probability density functions (PDFs) of grain motion variables typically ascribe an exponential-like distribution to grain velocity u_g with narrow tails (Furbish et al., 2016; Lajeunesse et al., 2010; Roseberry et al., 2012). Notably, certain studies identify a Gaussian-like core (Martin et al., 2012; Ancey & Heyman, 2014; Heyman et al., 2016), which may be attributed to experimental flow conditions or measurement methodology (Shim & Duan, 2019; Z. Wu et al., 2020; Yadav et al., 2026). This distribution dichotomy (a Gaussian core and exponential tail) is purportedly due to the mixture of both short and long grain flights, with long trajectories contributing Gaussian-like characteristics to the PDF of grain velocities. The combination of short and long flights and corresponding travel times of grain trajectories may also lead to the Weibull-like core and exponential-like tail that has been observed in distributions of bedload flight distances L_x (Z. Wu et al., 2020). Although common probability distributions are frequently used to describe bedload flight distance and travel time PDFs—typically the exponential distribution for travel times and exponential or Weibull distribution for flight distances (S. L. Fathel et al., 2015; Martin et al., 2012; M. X. Liu et al., 2019)—recent work by Z. Wu et al. (2023) propose an analytical solution for bedload flight statistics derived from Taylor dispersion theory.

Despite recent advances in high-speed imaging and automated grain-tracking methodologies, there remains a dearth of high-resolution datasets that describe both "bulk" grain statistics (i.e., grain activity, instantaneous grain velocities, and accelerations—metrics based on the collective behavior of identified grains) as well as the corresponding "trackwise" statistics (i.e., bedload flight distances, travel times, and grain rest times—metrics that rely on the discernment of individual grain trajectories). Notably, the experiments initially conducted by Roseberry et al. (2012), whose results were re-analyzed by S. L. Fathel et al. (2015) and have been used to validate many subsequent theoretical and numerical studies (Fan et al., 2014, 2016; Furbish et al., 2016, 2017; S. Fathel et al., 2016; Z. Wu et al., 2020, 2021, 2023), are restricted to trajectories extracted from videos with either a limited field of view or a short duration due to experimental constraints. Although additional work has been done to collect measurements of bedload movement statistics (Campagnol et al., 2013; M. X. Liu et al., 2019; Lajeunesse et al., 2010; Shim & Duan, 2017, 2019; Rebai et al., 2024; Salevan et al., 2017; C. Liu et al., 2024), we note that these studies almost entirely measured bedload flight statistics above the threshold of motion and many were constrained to the bulk grain metrics described above. The inclusion of trackwise statistics is, however, fundamental for the "entrainment form" parameterization of sediment flux, and for linking the advective and diffusive regimes. Furthermore, grain motion persists below the critical Shields stress; however, the intermittent sediment transport dynamics of a sub- or near-threshold system produce different sediment flux distributions compared to systems sufficiently above the threshold of motion (Benavides et al., 2022, 2023), demonstrating the need for observations at and below this critical transition.

In this study, we examine the motions of natural sand grains exposed to a turbulent shear flow. We collect images of the sand bed at high spatial and temporal resolutions, enabling us to extract particle trajectories for a range of flow conditions. We then segment the grain tracks into periods of motion and rest to extract the statistical distributions associated with the movement of grains as bedload. These variables include grain activity, velocity, acceleration, flight distance, and flight travel time. As previously mentioned, many studies have examined statistical descriptions of bedload motion using experimental data (Roseberry et al., 2012; S. L. Fathel et al., 2015; M. X. Liu et al., 2019; Rebai et al., 2024; Z. Wu et al., 2020; Shim & Duan, 2019, 2017; Lajeunesse et al., 2010) but are frequently limited in spatial or temporal extent, constrained to an above-threshold flow regime, or measure only bulk grain statistics; we add to these results with a robust dataset that spans nine bed stress intensities ranging from below the nominal critical Shields stress where grain movement is extremely intermittent ($\tau_*/\tau_{*cr} = 0.78$) to well above the onset of bulk sediment motion ($\tau_*/\tau_{*cr} = 1.53$). We perform eight replicates at each bed stress intensity. By including flow conditions below onset, we provide new insight about grain behavior in this highly intermittent regime of sediment transport and suggest that current assumptions for appropriate distributions for bedload flight travel time may break down in the very low transport state.

The rest of this paper is structured as follows. After an overview of our experimental setup and protocols in Section 2, we describe the implementation of a hidden Markov model that identifies periods of motion and rest in grain trajectory timeseries in Section 3. We justify the use of machine learning techniques by comparing our model with previous methods for identifying grain motion, and discuss the underlying assumptions. In Section 4, we present our results—organized according to grain-motion variable—as well as additional discussion of the proposed probability distributions in relation to previous work. These results are followed by a broader discussion and summary in Part 5. Subsequently, in a companion paper, we use the methodology and statistical descriptions validated here to investigate the effects of directional stress history on bedload motion (Bodek, Wang, Shattuck, O'Hern, & Ouellette, 2026b).

2 Experimental Methods

2.1 Configuration and Procedure

The experimental data analyzed here was initially collected by Bodek, Wang, Shattuck, O'Hern, and Ouellette (2026a), who used a recirculating, open channel flume at the Environmental Fluid Mechanics Laboratory at Stanford University. This flume had a rectangular channel of length 6 m and width 0.6 m, with a 3 m glass-walled test section in which measurements were taken. A full description of the flume facility is documented in O'Riordan et al. (1993).

A sediment bed was installed into the channel floor 1.3 m from the entrance of the test section and centered within the channel cross section. This inset sediment bed consisted of a circular dish that was 45.7 cm (18 in) in diameter and 7.6 cm (3 in) deep; this dish was positioned such that the edge was flush with the surrounding smooth acrylic channel floor. The sediment itself consisted of medium to coarse-sized quartz sand (D_{50} = 0.495 mm; $\rho_s = 2650$ kg/m^3). The sand was sieved to constrain the minimum and maximum grain sizes (0.3 mm to 0.8 mm) and to produce a uniform grain size distribution with $\sigma_g = (D_{84}/D_{16})^{0.5} = 1.24$, as measured using a Camsizer X2 instrument (García, 2013).

A downward-facing camera was mounted above the center of the sediment bed to record the motion of sand grains; a small glass window was placed on the free surface of the flow above the sediment bed to ensure that distortions of the flow surface did not impede the view of the sand below. An acoustic Doppler profiling velocimeter (ADV) was mounted behind this window over the downstream portion of the sediment bed to collect flow velocity measurements and characterize the friction velocity u_*, bed stress τ_b, and Shields stress, or non-dimensional bed stress $\tau_* = \tau_b/[(\rho_s - \rho)gD_{50}]$, where $\rho =$ 1000 kg/m^3 is the fluid density, ρ_s is the sediment density, g is the gravitational acceleration, and D_{50} is the median grain size. Measurements of u_*, τ_b, and τ_* were collected at 9 settings of the variable-speed pump that ranged from below critical $\tau_*/\tau_{*cr} = 0.78$ to above the onset of grain motion $\tau_*/\tau_{*cr} = 1.53$. The flow depth at rest was 17.5 cm. Although the fluid flow deepened as the discharge increased due to the fixed height of the control weir, the water depth in the channel varied by less than 4 cm over the range of flow rates used in the experiments. These experiments were conducted in hydraulically transitional flow with particle Reynolds number $Re_p = u_* D_{50}/\nu$ ranging from $Re_p =$ 6.8–10.6 for our flow settings, where the kinematic viscosity of water is approximately $\nu = 10^{-6}$ m^2/s. The nominal critical value Shields stress, $\tau_{*cr} \approx 0.033$, was estimated by plotting τ_* and Re_p determined for various flow rates on the Shields curve (Vanoni, 2006), then interpolating the τ_{*cr} value where these points and the Shields curve intersect.

The sediment bed was prepared prior to each experiment using the same protocol. The submerged sand bed was first agitated using a stirring implement, then leveled by dragging a stiff piece of mesh over the bed surface in the downstream direction. Next, the flow rate was increased in a series of 9 step-ups of the variable-speed pump. After each increase in pump output, the flow was allowed to stabilize for 1 min, after which a 45 sec video of the sediment motions was collected. The increasing step-ups in flow rate occurred over approximately 19 min, as each flow rate also included a 15–20 second adjustment time needed to change the variable-speed pump. The relatively rapid increase in bed stress ensured that the sediment bed did not substantially change its surface elevation, as only the highest flow rates (corresponding to $\tau_* = 0.048$ to 0.05) were capable of inducing scour or initiating bedforms. Even then, these features were constrained to the edges of the sediment bed and outside the field of view of the camera. The sediment transport regime in the flume was limited to bedload; the grains were not observed to travel in suspension during these experiments. The bed was always reset before any new experiment was conducted; thus, observations of sediment motion were made on a newly prepared bed. A total of 8 independent trials were conducted.

2.2 Sediment Bed Imaging and Particle Tracking

The grain motions were imaged using a downward-facing Flea3 monochrome camera (model FL3-U3-13Y3M-C manufactured by Teledyne FLIR) with an SMC Pentax-M 28 mm f2.8 lens that was mounted above the center of the sediment bed looking through the glass window onto a 10.9 cm$\times$8.75 cm field of view. Images measuring 1280$\times$1024 pixels with a spatial resolution of 0.085 mm per pixel were captured at 120 frames per second. To facilitate particle identification, a sub-population of grains was spray-painted fluorescent orange and mixed with the unpainted sand in a 17/83 mixture by volume. These grains glowed when illuminated by an ultraviolet light in a dark room; further, the camera lens was fitted with an optical band pass filter to collect light emitted by the paint, resulting in the painted sub-population of grains appearing bright on the dark background of unpainted sand (Figure 1a).

We reconstructed the particle trajectories of the fluorescing grains using a multi-frame predictive particle-tracking algorithm (Ouellette et al., 2006); grain velocities and accelerations were then computed from these trajectories via convolution with a smoothing and differentiating kernel (Mordant et al., 2004). Particle tracking has been used to characterize grain behavior in numerous other sediment transport studies (e.g., Salevan et al., 2017; Lajeunesse et al., 2010; Shim & Duan, 2017; Radice et al., 2017). Parameters specified for the tracking algorithm of Ouellette et al. (2006) included a threshold intensity such that approximately 800 grains were identified in each frame, as well as a minimum and maximum particle area corresponding to the smallest and largest grain sizes. While this algorithm kinematically predicts particle trajectories over multiple frames, we specify a search radius in the predicted particle position if the tracked grain is not immediately found. A suitable search radius was iteratively selected using manual visual inspection to check for track accuracy (Figure 1a). We note that the tracking algorithm of Ouellette et al. (2006) breaks tracks when a conflict arises (i.e., more than one identified particle is the most likely next match for multiple trajectories); thus, false tracks are highly unlikely to occur.

3 Grain Trajectory Analysis

3.1 Implementation of the Hidden Markov Model

When examining the trajectories of individual sediment grains, it becomes necessary to distinguish between periods of flight and rest. While these states are often readily identifiable using manual visual inspection (see Figure 1), many automated definitions rely on a prior selection of parameters, typically a threshold velocity or distance

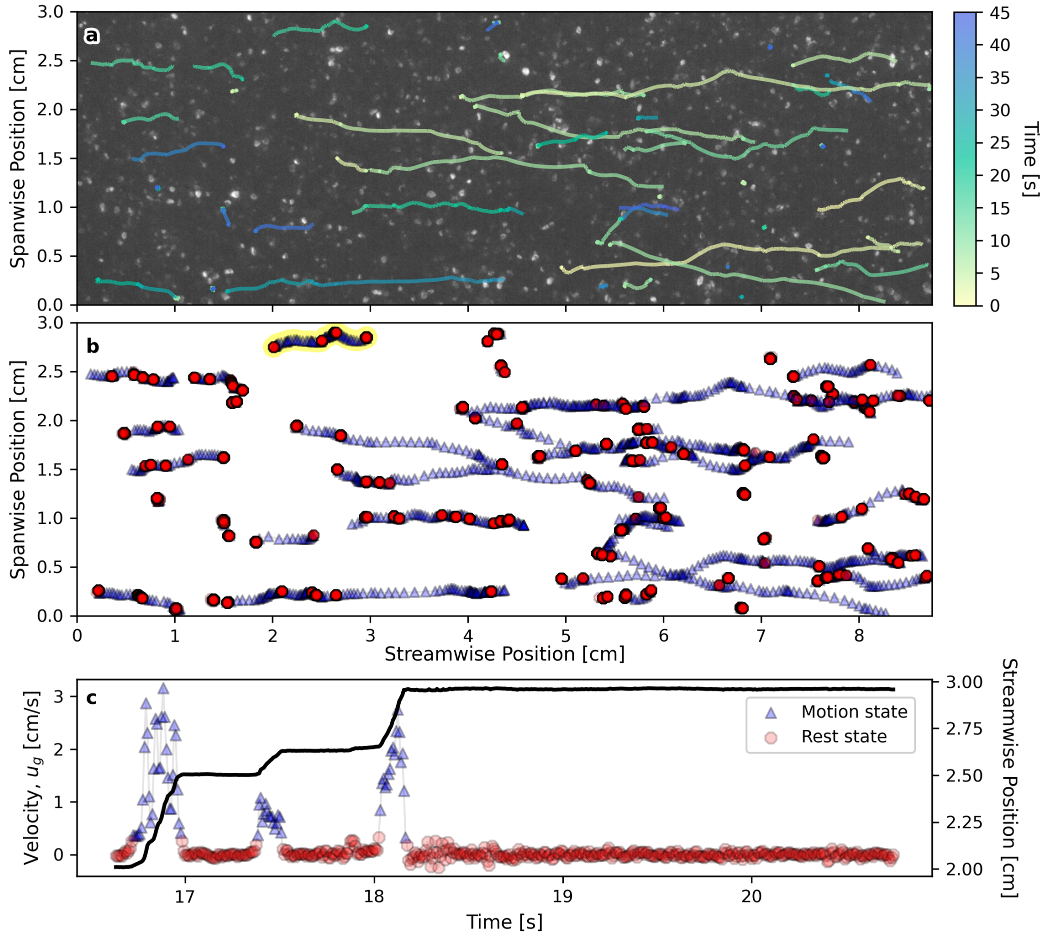

Figure 1. (a) Example sediment trajectories from the particle-tracking analysis overlaid onto an image of the underlying sediment bed; note the appearance of fluorescing sand grains illuminated by the ultraviolet light. These trajectories represent transport conditions over a subset of the sediment bed at $\tau_* = 0.039$, $\frac{\tau_*}{\tau_{*cr}} = 1.2$. Time is reported through color coding with respect to the start of the 45 sec video; the flow direction is from left to right. (b) The same sediment trajectories as depicted in panel (a) with markers indicating periods of motion (blue) and rest (red); the yellow-highlighted track is further examined in panel (c). (c) Timeseries of streamwise position (black line) and velocity (red/blue markers) for one example trajectory illustrating segments of motion and rest as identified using a hidden Markov model.

traveled (e.g., González et al., 2017; M. X. Liu et al., 2019; Martin et al., 2012). In recent years, data-driven approaches have been proposed to predict bedload transport rates (e.g., Bhattacharya et al., 2005), including the use of Markov chains in sediment transport modeling (F.-C. Wu & Yang, 2004; Sun & Donahue, 2000). Markov chains describe a stochastic process with a Markov property (i.e., memorylessness)—so that, conditional on the current state of the system, the future and past states are independent (Markov, 1913). In other words, the probability of transitioning to a future state depends only on the current state, not on the sequence of states that preceded it. A hidden Markov model (HMM) describes a *hidden* Markov process that can be predicted using ordered observational data (Baum & Petrie, 1966; Baum & Eagon, 1967). The model specifically consists of a Markov chain governing transitions between hidden states and an emission model that generates observations based on the current hidden state. In our use case, we use observations of grain velocity obtained from the particle tracking analysis to predict whether the sediment grains are instantaneously in a hidden state of motion or rest along their trajectories (Figure 1b, 1c). Hidden Markov models have many varied uses due to their ability to describe state changes and are frequently used in signal processing and pattern recognition (e.g., Rabiner, 1989; Ephraim & Merhav, 2002), bioinformatics (e.g., Eddy, 1996; Krogh et al., 1994), economics and finance (e.g., Hamilton, 1989), and many other fields. HMMs also have use cases in the Earth and environmental sciences with applications to runoff predictions (e.g., Thyer & Kuczera, 2003), water quality analysis (e.g., Li et al., 2022), and—as previously mentioned—sediment transport modeling.

To implement this HMM for bedload state prediction, we use the *hmmlearn* Python library with a custom emission distribution for observations of streamwise grain velocity (Cournapeau et al., 2024). We specified a mixture model for instantaneous grain velocity observations consisting of a Student's t and exponential distributions, with the peaked Student's t core attributed to fluctuating near-zero velocities of grains at rest or jiggling in place and a decaying exponential at higher velocities representing grains actively moving as bedload (Salevan et al., 2017; Galanis et al., 2022; Bodek, Wang, Shattuck, O'Hern, & Ouellette, 2026a; Rebai et al., 2024; González et al., 2017). We then trained the model using the Baum-Welch expectation-maximization algorithm to estimate HMM parameters (Baum, 1972), and decoded the most likely hidden state sequence using the Viterbi algorithm (Viterbi, 1967). We used manual visual inspection of track positions to verify the accuracy of the predicted hidden states (Figure 1c). Subsequently, we adjusted the likelihood of each hidden state by setting a higher threshold for the motion state based on the posterior probabilities (i.e., the probability that an observation belongs to a hidden state) to better match visual observations of motion and rest. Once trajectories were segmented into the motion and rest states, we could then calculate flight distance and flight duration based on the time difference and streamwise and spanwise grain displacement from the start to the end of a motion segment. We only considered completed grain flights (i.e., grain flights that are bookended with the rest state) to avoid truncated flights that either left the field of view or whose trajectories were not completed.

3.2 Efficacy of the Hidden Markov Model

We propose the hidden Markov model as a suitable method for differentiating between motion and rest in observational data of bedload transport that improves on previous methods. As mentioned above, many automated definitions rely on a prior selection of parameters or are constrained by the experimental imaging setup, typically the spatial or temporal camera resolution. For example, prior studies have often categorized a flight as a period when the grain velocity exceeds a specified threshold (González et al., 2017; Yadav et al., 2026); the selection of this velocity threshold, however, cannot be determined from first principles and impacts subsequent analysis (Salevan et al., 2017). In other cases, experimental limitations result in a similar cutoff threshold when subtle grain motions cannot reliably be measured (Lajeunesse et al., 2010). These definitions may incorporate a spatial dimension as well, where grains must travel some fraction of their grain diameter while their velocity exceeds this threshold (M. X. Liu et al., 2019). Other definitions rely entirely on distance traveled over a measurement timestep (Martin et al., 2012; Cecchetto et al., 2018), or simply require that the grain continues to make forward progress (Campagnol et al., 2013, 2015). A major consequence of this threshold selection is the shape of the resulting PDF of instantaneous streamwise grain velocities and grain activity. Z. Wu et al. (2020) demonstrate that the grain velocity PDF transitions from an exponential to a truncated Gaussian-like distribution when short grain flights (based on flight travel time, but correlated with lower grain velocities and shorter flight distances) are excluded. Similarly, Salevan et al. (2017) demonstrated that increasing the threshold velocity for grain activity produces a qualitative transition in the PDF of the grain activity fraction n_{active} from a truncated Gaussian-like distribution to an exponential-like distribution. Given the sensitivity of both grain activity and velocity distributions to threshold selection, a more reliable and less subjective method for distinguishing between grain motion and rest is crucial for accurate parameterization of the "activity form" of sediment flux.

Additionally, periods of rest are often defined based on disentrainment (i.e., the grain velocity falling below the velocity threshold) for a specified duration (Cecchetto et al., 2018) or failure to travel some fraction of a grain diameter over a specified amount of time (Martin et al., 2012). The selection of this minimum rest time or disentrainment velocity is also arbitrary, and impacts whether low-velocity segments of grain trajectories are considered merely collisions with the bed or an actual period of rest. The grain rest time distribution is fundamental to characterizing the diffusion regime of bedload tracer particles at different spatiotemporal scales—typically described as the local (successive particle-bed collisions), intermediate (motion between successive periods of rest), and global ranges (trajectories consisting of multiple flights and rest periods) (Nikora et al., 2002). The diffusion regime during the intermediate and global ranges can vary based on unique conditions imposed by the hydrologic regime or sediment bed configuration; heavy-tailed distributions of rest time imply subdiffusive behavior as grains are trapped within the sediment bed for long periods, while exponential or light-tailed distributions may occur due to correlated grain motion and imply superdiffusion (Martin et al., 2012; Nikora et al., 2002; Ganti et al., 2010; Schumer et al., 2009).

The hidden Markov model improves on previous threshold-based approaches by using unsupervised classification to identify periods of motion and rest. The HMM is trained using the instantaneous velocity distribution of *all* identified grains; by specifying that grains at rest follow a Gaussian-like (specifically, Student's t) distribution and grains in motion follow an exponential distribution (Salevan et al., 2017), the decoding of trajectories into motion and rest states is specific to the flow conditions during each data collection run. This two-state model aligns with commonly observed grain velocity PDFs in studies that examine the full distribution of instantaneous grain velocities (Galanis et al., 2022; Bodek, Wang, Shattuck, O'Hern, & Ouellette, 2026a; Rebai et al., 2024; González et al., 2017). This method expands the approach used by Bodek, Wang, Shattuck, O'Hern, and Ouellette (2026a), who selected a variable threshold based on the grain velocity where the relative contribution of the Student's t distribution and exponential distribution are equal.

Additionally, while Markov chains are "memoryless," the transition probability structure allows for a "smoothing" of the velocity signal. The transition probability that a grain changes state is constant per unit time. This constraint makes rapid changes between states extremely unlikely under the model. As a result, grains in motion remain in the motion state through brief low-velocity fluctuations—for instance, when a grain collides with the bed but continues moving downstream—and similarly allows grains at rest to remain in the rest state despite brief high-velocity fluctuations while jiggling in place.

Finally, we note that even though HMMs are frequently used for analyzing time-series and classifying systems even when the underlying process does not follow Markov chain assumptions (Rabiner, 1989), bedload dynamics offers strong theoretical justification for the Markov framework. For individual grains undergoing bedload transport, the transition between motion and rest is random and it is frequently assumed that particle movement (or lack thereof) is influenced only by its present state (Lisle et al., 1998; Papanicolaou et al., 2002). Notably, Ancey et al. (2006) modeled the movement of a sediment grain as bedload using a two-state Markov process (specifically the telegraph process), where state transitions occur with constant probability per unit time, resulting in exponentially distributed grain flight times and wait times. This approach mirrors the hidden Markov model implementation, which utilizes a constant probability of transitioning between motion and rest states when decoding individual trajectories. We identify an exponential distribution of grain flight times for flow conditions above the threshold of motion (see Section 4.2), as is expected from a telegraph process. However, the assumption of a telegraph process breaks down when generalized to multiple grains in an observation window (Ancey et al., 2006). Grain activity is observed to display a negative binomial-like distribution in our (see Section 4.1) and other studies (e.g., Ancey et al., 2006; González et al., 2017), indicating that the constant-rate assumption fails to capture collective entrainment effects where particle motion exhibits state-dependent correlations (Ancey, 2010; Ancey et al., 2008; Ancey & Heyman, 2014).

3.3 Entrainment Probability

The transition matrix is an HMM parameter that indicates the probability of transitioning between states, which we estimate using the Baum-Welch algorithm implemented by *hmmlearn*. The probability that a grain transitions from the rest state to the motion state is, in essence, an entrainment probability. Estimates and parameterizations of entrainment probability have long been of interest to those studying bedload transport and are typically expected to be a function of Shields stress. Einstein (1950) proposed an entrainment function based on an assumption of a Gaussian probability distribution for the fluctuating hydrodynamic lift acting on a particle to exceed its submerged weight. Subsequent contributions involve alternate distributions for the fluctuating instantaneous streamwise fluid velocities, configuration of grains on the sediment bed, and different modes of downstream transport (i.e., rolling or lifting) (F.-C. Wu & Lin, 2002; F.-C. Wu & Chou, 2003; Cheng & Chiew, 1998). The entrainment of sediment particles is, therefore, characterized by the probability of the near-bed instantaneous streamwise fluid velocity at the level of an individual grain relative to the grains on the bed and their alignments with the streamwise direction.

We validate our HMM-based entrainment probabilities by comparing with previous experimental data (Guy et al., 1966; Luque & Erosion, 1974; Papanicolaou et al., 2002; Jain, 1992), the empirical formula of Fredsoe and Deigaard (1992), and the initially proposed function of Einstein (1950) (Figure 2). We observe good agreement for HMM-based entrainment probabilities at and in excess of the critical Shields stress ($\tau_* \geq 0.033$), noting that higher bed stress conditions ($\tau_* \geq 0.045$) fall along the empirical prediction of Fredsoe and Deigaard (1992). Intermediate bed stresses only slightly in excess of the critical Shields stress ($0.034 \leq \tau_* \leq 0.042$) fall between the Einstein (1950) and Fredsoe and Deigaard (1992) predictions. Most notably, the entrainment probabilities estimated by the HMM deviate from expected trends below the critical Shields stress ($\tau_* \leq 0.030$) based on previous experimental data and empirical estimates.

We observe the HMM does not fit the data well at the lowest bed stress conditions, which should display the smallest entrainment probabilities. For these sub-threshold flows, we found that the HMM had a tendency to over-predict the motion state leading to higher than expected entrainment probabilities. Since we enforce a two-state model for the grain velocities, it is likely that the positive tail of the Student's t distribution was attributed to the supposedly moving exponentially-distributed grains. This resulted in temporary higher-velocity jiggles being categorized as periods of motion, when visual verification revealed no significant downstream movement. The over-prediction of grain jiggles as belonging to the motion state likely accounts for the unexpectedly high entrainment probabilities observed for sub-threshold flow conditions. We addressed this over-prediction by examining the posterior probabilities (i.e., the probability that an observation belongs to a hidden state) and adjusting the likelihood of an observation being attributable to the motion state. This adjustment successfully reduces the false categorization of brief high-velocity jiggles into the motion state, but does not alter the underlying transition matrix and entrainment probabilities reported in Figure 2.

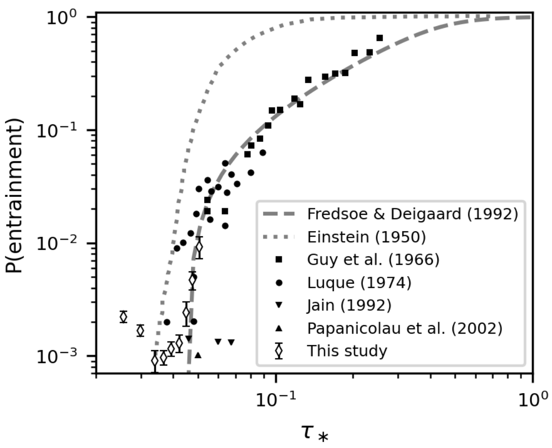

Figure 2. Entrainment probability as identified by the HMM transition matrix as a function of Shields stress τ_*. Probabilities determined from our experiments (white diamonds) are shown in comparison to previous estimates from other experimental studies and entrainment probability calculation criteria. Error bars indicate 95% confidence intervals computed for eight trials.

4 Probabilistic Descriptions of Grains in Motion

4.1 Grain Activity

To quantify grain activity, we can simply count the number of active grains (i.e., grains in the motion state) in a given frame. We report this grain activity metric as an "activity fraction"—the ratio of moving grains to all grains identified in each frame (Salevan et al., 2017). This metric is similar to the surface density of moving particles as introduced by Lajeunesse et al. (2010) or the particle activity used by Roseberry et al. (2012), although we note that these grain activity measurements normalize by unit surface area. We can see that the mean grain activity fraction $\langle n_{active} \rangle$ increases as a function of Shields stress (Figure 3a), as expected. Furthermore, if we treat each frame as an instantaneous sample of the number of active grains N_g, we can then generate a probability density function (PDF) of the count of instantaneously active grains for increasing Shields stresses (Figure 3b–3e). We observe that for Shields stresses at and below the threshold of motion, the grain activity PDFs appear exponential-like and are dominated by counts of 0 or 1 moving grains (Figure 3b, 3c), while the PDFs begin to exhibit more lognormal or normal appearances once the threshold of motion is exceeded and greater numbers of grains are entrained (Figure 3d, 3e). This shift from exponential-like to Gaussian-like has previously been observed and described using the discrete negative binomial distribution (Ancey et al., 2006) or continuous Gamma distribution (González et al., 2017). This transition reflects the shift from highly intermittent, uncorrelated grain motions near threshold to more collective entrainment effects and a greater quantity of moving grains at higher bed stresses.

4.2 Grain Velocities

The instantaneous streamwise velocities of grains moving as bedload (based on categorization into the motion state) are well described using an exponential distribution (Figure 4a), as given by

$$P(u_g) = \frac{1}{\langle u_g \rangle} e^{-\frac{u_g}{\langle u_g \rangle}}, \qquad u_g \geq 0 \tag{1}$$

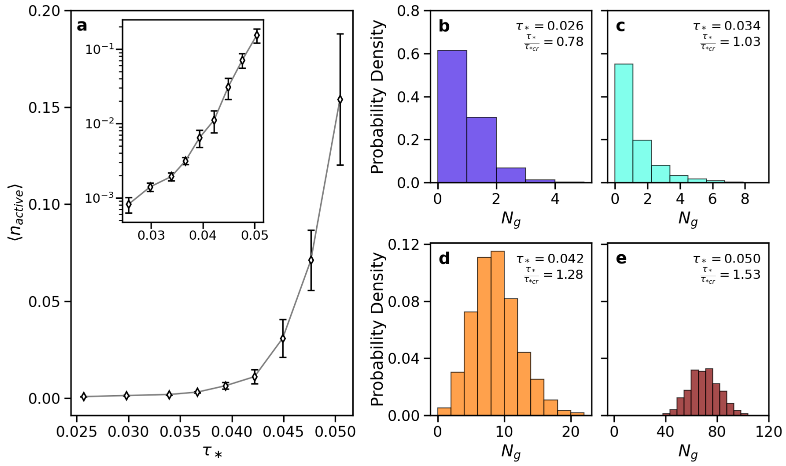

Figure 3. (a) Mean grain activity fraction $\langle n_{active} \rangle$ as a function of Shields stress τ_*; the inset shows same data plotted on semi-logarithmic axes and error bars show 95% confidence interval computed for eight trials. (b–d) PDFs of the number of active grains N_g in each frame of a video of the sediment bed for one trial; each panel depicts bed activity at four flow velocity intervals with τ_* and $\tau_*/\tau_{*\,cr}$ reported.

where $\langle u_g \rangle$ is the average streamwise velocity. Similarly, the spanwise grain velocity distribution can be described using a two-sided exponential distribution (also known as a Laplace distribution) that is symmetric about $v_g = 0$ cm/s (Figure 4b), as given by

$$P(|v_g|) = \frac{1}{|\langle v_g \rangle|} e^{-\frac{|v_g|}{|\langle v_g \rangle|}} \tag{2}$$

where $\langle v_g \rangle$ is the average spanwise velocity in one cross-stream direction; when both directions are considered, $\langle v_g \rangle \approx 0$ cm/s. These observations of instantaneous streamwise and spanwise grain velocities are consistent with prior studies (Lajeunesse et al., 2010; Roseberry et al., 2012; S. L. Fathel et al., 2015; Yadav et al., 2026). Our collected data also agrees with theory, where the exponential distribution can be derived from maximum-entropy statistical-mechanical arguments, starting from a microcanonical ensemble and constraining the total grain momentum (Furbish & Schmeeckle, 2013). Using the best-fit exponential distribution to determine mean streamwise and spanwise grain velocity, we find that both $\langle u_g \rangle$ and $\langle v_g \rangle$ increase as a function of Shields stress (Figure 4c).

Additionally, we note that for small particle numbers, the distribution of velocities is expected to be exponential-like but with a less heavy tail (Furbish & Schmeeckle, 2013; S. L. Fathel et al., 2015). We observe this behavior for streamwise velocities at transport conditions above the threshold of motion (see the $\tau_* = 0.048$ and $\tau_* = 0.05$ case in Figure 4a), suggesting that near-bed fluid velocities act as a control on the maximum particle velocity in this regime. Notably, we do not observe this light-tailed behavior for spanwise grain velocities at any of the flow settings (Figure 4b), despite parallel expectations (Furbish & Schmeeckle, 2013). It appears that M. X. Liu et al. (2019) may also observe heavier-than-expected tails in their spanwise grain velocity distributions.

We also find that streamwise grain velocity distributions deviate from the expected light-tailed or strictly exponential behavior for critical and sub-critical flow conditions. In the sub-critical to critical regime, u_g tends to be more peaked than an exponential distribution and with heavier tails (see the $\tau_* = 0.026$ to $\tau_* = 0.034$ cases in Figure 4a). In the highly intermittent regime of sub-threshold flow, these distributions may cap-

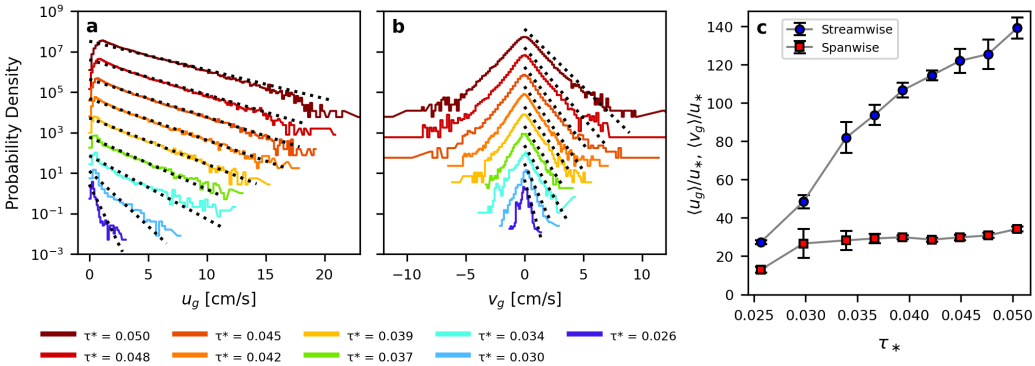

Figure 4. (a) PDF of streamwise grain velocities u_g for one trial; dotted lines are best fits to an exponential distribution. (b) PDF of spanwise grain velocities v_g; dotted lines are best fits to an exponential distribution for positive v_g values. For clarity, the PDFs in panels (a) and (b) are vertically shifted by a factor of 10 from each other. The cyan-colored line is the experimental condition closest to the nominal onset of motion ($\tau_* = 0.034$, $\tau_*/\tau_{*\,cr} = 1.03$). (c) Mean streamwise and spanwise grain velocities, normalized by friction velocity u_*, as a function of Shields stress τ_*; the normalizing factor u_* also increases as a function of τ_*. Error bars show 95% confidence intervals computed for eight trials.

ture a bimodality of grain motion—a combination of short, slow displacements (e.g., grains rolling out of pockets then stopping again) interspersed with longer flights as a grain occasionally encounters an energetic turbulent structure and becomes entrained into the flow.

4.3 Grain Accelerations

The instantaneous streamwise and spanwise accelerations of grains moving as bedload are typically both described using a two-sided exponential distribution—that is, a Laplace distribution—centered about $a_{x\,g} = 0$ m/s^2 (S. L. Fathel et al., 2015; M. X. Liu et al., 2019; Furbish et al., 2016). Based on our observations, we find good agreement between the streamwise acceleration PDFs and the Laplace distribution (Figure 5a). Spanwise acceleration distributions also appear Laplace-like for flow conditions at and below the critical Shields stress; however, the PDFs of $a_{y\,g}$ begin to display heavier-than-exponential tails once the critical Shields stress is exceeded (Figure 5b). The distribution of spanwise grain accelerations is infrequently reported; however, we note that S. L. Fathel et al. (2015) find an that exponential distribution fit their spanwise acceleration observations well.

For "equilibrium" sediment transport, the ensemble average of streamwise grain accelerations must be zero (Furbish, Roseberry, & Schmeeckle, 2012), which we observe: for both streamwise and spanwise acceleration, the PDFs are centered at 0 m/s^2. Interestingly, however, when we compute the skewness of the streamwise acceleration distributions, we find that these PDFs have a negative skewness for flow conditions below the threshold of motion, but positive skewness once flow conditions exceed the critical Shields stress (Figure 5c).

We hypothesize that the negative skewness observed for sub-critical flow conditions is due to flight-crash dynamics—relatively gentle accelerations followed by rapid decelerations as grains "crash" into the sediment bed. Flight-crash dynamics are observed in

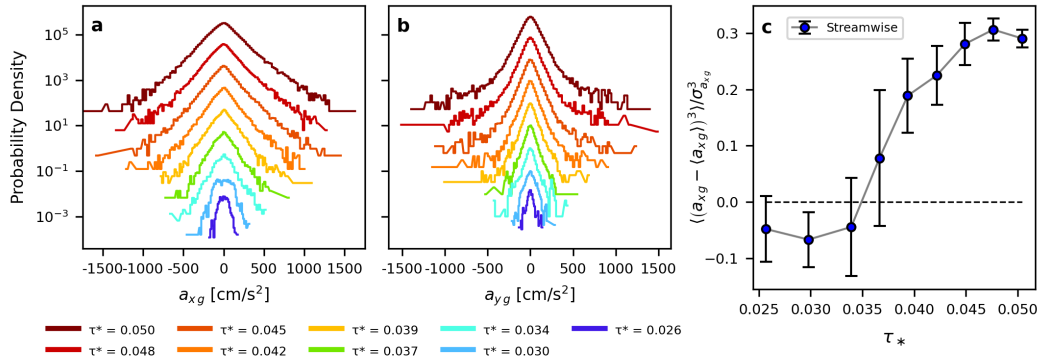

Figure 5. (a) PDF of streamwise grain accelerations $a_{x\,g}$ for one trial. (b) PDF of spanwise grain accelerations $a_{y\,g}$. For clarity, the PDFs in panels (a) and (b) are vertically shifted by a factor of 10 from each other. The cyan-colored line is the experimental condition closest to the nominal onset of motion ($\tau_* = 0.034$, $\tau_*/\tau_{*\,cr} = 1.03$). (c) Mean skewness of streamwise acceleration distributions as a function of Shields stress τ_*; error bars show 95% confidence interval computed for eight trials, while the horizontal dashed line represents a skewness of zero indicating a symmetric distribution.

turbulence (Xu et al., 2014; Švančara & La Mantia, 2019), as well as in traffic and financial markets (Helbing, 2001; Jensen et al., 2003). At flow conditions that exceed the threshold of motion, we see the opposite phenomenon—a "lift and settle" effect where grains accelerate rapidly as they are lifted off the bed then gently decelerate as they return to rest. It is possible that grain motions at higher flow velocities are dominated by turbulent sweeps or ejection events (e.g., Lelouvetel et al., 2009) and become disentrained due to encountering a patch of low velocity fluid, rather than due to violent collisions with the bed.

4.4 Grain Flight Times

Grain travel time—that is, the time over which a completed flight occurs—is frequently described using an exponential distribution (Figure 6a), as given by

$$P(T_f) = \frac{1}{\langle T_f \rangle} e^{-\frac{T_f}{\langle T_f \rangle}}, \qquad T_f \geq 0 \tag{3}$$

where $\langle T_f \rangle$ is the mean flight time. This hypothesis is supported by both experimental (Martin et al., 2012; M. X. Liu et al., 2019) and numerical (Z. Wu et al., 2020) observations, and is theoretically justified assuming a constant disentrainment rate (Furbish et al., 2016; Ancey et al., 2006). We observe that mean flight time, as determined using the best-fit exponential distribution, increases as a function of Shields stress, but begins to plateau as $\tau_* \geq 0.045$ (Figure 6c).

While grains flight times are well approximated by an exponential distribution for flow conditions above the critical Shields stress, we observe PDFs that appear more peaked than an exponential and with heavier tails for flight durations at and below the critical flow condition (see Figure 6a for $\tau_* \leq 0.039$). This result suggests that the assumption of a constant disentrainment rate breaks down in the sub- and near-threshold regime.

Although the exponential distribution is frequently used to characterize these statistics, we also considered a recent study by Z. Wu et al. (2023) who proposed an analytical solution for distributions of grain flight times and distances traveled. The Z. Wu et

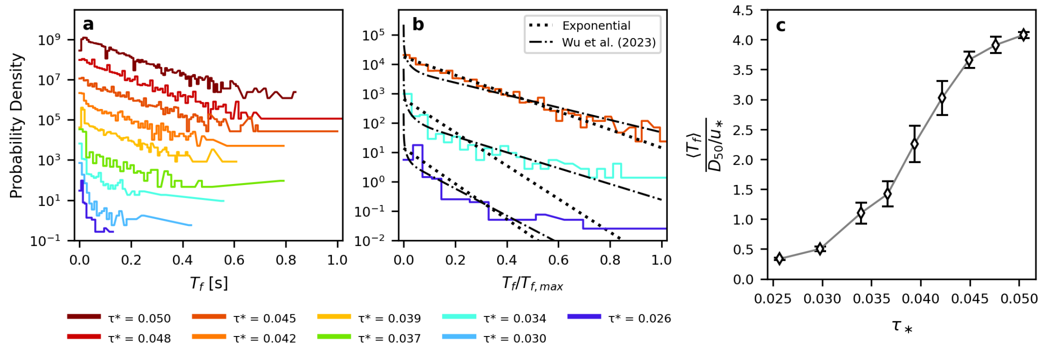

Figure 6. (a) PDF of grain flight travel time T_f for one trial; for clarity, the PDFs are vertically shifted by a factor of 10 from each other. (b) PDF of grain travel time T_f for three flow conditions: below onset ($\tau_* = 0.026$, $\tau_*/\tau_{*\,cr} = 0.78$ shown with the dark blue solid line), at onset ($\tau_* = 0.034$, $\tau_*/\tau_{*\,cr} = 1.03$ shown in cyan), and above the threshold of motion ($\tau_* = 0.045$, $\tau_*/\tau_{*\,cr} = 1.36$ shown in orange). The horizontal axis is normalized by the maximum flight time $T_{f\,max}$ and PDFs are vertically shifted by a factor of 50 for ease of visual comparison of each PDF to an exponential distribution (dotted lines) and the distribution of Z. Wu et al. (2023) (dash-dotted lines). (c) Mean grain flight time, normalized by D_{50}/u_*, as a function of Shields stress τ_*; error bars show 95% confidence intervals computed for eight trials.

al. (2023) flight time distribution appears—at least qualitatively—to display a Weibull-like core and exponential-like tail, which match our observations, especially for the near-threshold cases. We can apply the Z. Wu et al. (2023) distribution to our PDFs using a maximum likelihood estimation (MLE) algorithm and observe good visual agreement, especially when compared to the best-fit exponential distribution (Figure 6b). Additionally, the parameters of the Z. Wu et al. (2023) distribution represent physical quantities: the mean grain velocity, coefficient for velocity diffusivity, and deposition rate. When identifying the best-fit distribution to our data, we constrain the grain velocity parameter using a narrow envelope around our measured $\langle u_g \rangle$.

4.5 Grain Flight Distances

Particle flight lengths L_x and L_y are often described using the Weibull distribution (S. L. Fathel et al., 2015; Furbish et al., 2016; Yadav et al., 2026), as generalized for either streamwise or spanwise flight distances L_f:

$$P(L_f) = \frac{k}{\lambda}\left(\frac{L_f}{\lambda}\right)^{k-1} e^{-\left(\frac{L_f}{\lambda}\right)^k}, \tag{4}$$

where $k > 0$ is the shape parameter and $\lambda > 0$ is the scale parameter. When $k = 1$, the Weibull distribution approaches the exponential distribution. Based on the assumption that $L_x \propto T_f^2$, S. L. Fathel et al. (2015) derived a distribution for flight distances with a Weibullian form:

$$P(L_x) = \frac{\sqrt{2/\langle L_x \rangle}}{2L_x^{1/2}} e^{-\sqrt{2/\langle L_x \rangle} L_x^{1/2}}, \tag{5}$$

where $\langle L_x \rangle$ is the mean flight distance. This distribution is assumed to apply for both streamwise and spanwise flight distances, although fewer studies report spanwise measurements. Using the same scaling assumption $L_x \propto T_f^2$, S. L. Fathel et al. (2015) determined that the shape parameter should be $k = 0.5$ and scale parameter should be

$\lambda = \langle L_f \rangle/2$, although their experimental results found that $k = 0.67$ and 2λ did not match their measured mean streamwise flight distance. The shape parameter, as determined using a best-fit Weibull distribution to our flight distance data, ranges from $k =$ 0.40 (standard deviation 0.037) at the lowest flow condition ($\tau_* = 0.026$) to $k = 0.72$ (standard deviation 0.03) at one of the highest flow conditions ($\tau_* = 0.048$); there is also a lack of agreement between our measured $\langle L_x \rangle$ and twice the scale parameter λ. Although flight distance distributions are also described using the exponential distribution (M. X. Liu et al., 2019; Martin et al., 2012), we observe good agreement between both streamwise flight distance L_x and spanwise flight distance L_y and the Weibull distribution (Figure 7a, 7b). Additionally, we observe that mean streamwise and spanwise flight distance $\langle L_x \rangle$, $\langle L_y \rangle$ increase as a function of Shields stress (Figure 7d).

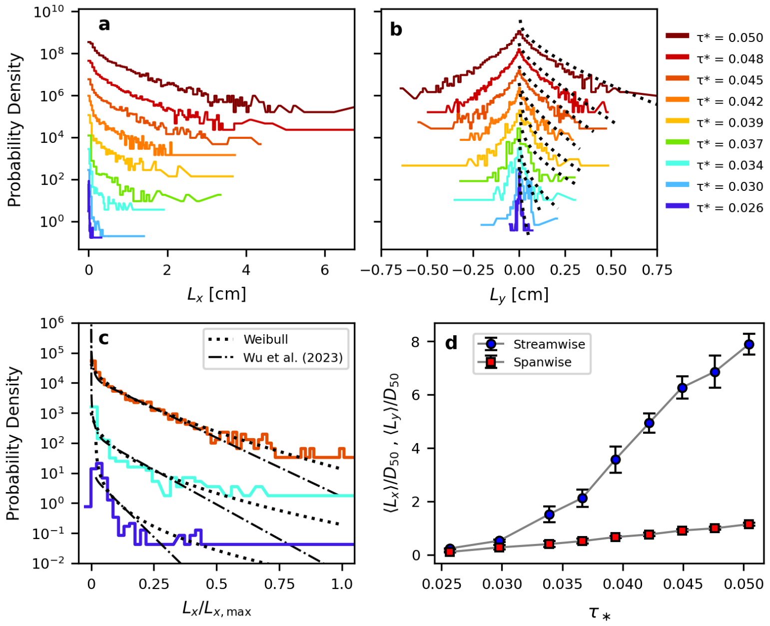

Figure 7. (a) PDF of streamwise grain flight distances L_x for one trial. (b) PDF of spanwise flight distances L_y; dotted lines are best fits to a Weibull distribution for positive values. For clarity, the PDFs in panels (a) and (b) are vertically shifted by a factor of 10 from each other. (c) PDF of spanwise flight distances L_x for three flow conditions: below onset ($\tau_* = 0.026$, $\tau_*/\tau_{*\,cr} = 0.78$ shown with the dark blue solid line), at onset ($\tau_* = 0.034$, $\tau_*/\tau_{*\,cr} = 1.03$ shown in cyan), and above the threshold of motion ($\tau_* = 0.045$, $\tau_*/\tau_{*\,cr} = 1.36$ shown in orange). The horizontal axis is normalized by the maximum flight distance $L_{x\,max}$ and PDFs are vertically shifted by a factor of 50 for ease of visual comparison of each PDF to an exponential distribution (dotted lines) and the distribution of Z. Wu et al. (2023) (dash-dotted lines). (d) Mean streamwise and spanwise flight distance, normalized by median grain size D_{50}, as a function of Shields stress τ_*; error bars show 95% confidence intervals computed for eight trials.

Notably, Z. Wu et al. (2020) suggest a Weibull distribution for shorter flights, but exponential for longer flights. Their argument is as follows. Grains in flight are more likely to be deposited (i.e., disentrained) close to where they began their trajectory; however, grains in flight experience a decreasing spatial disentrainment rate with increased hop distance (i.e., a grain in a long trajectory is less likely to be deposited) (Roseberry et al., 2012; Furbish, Haff, et al., 2012). This hypothesis supports a Weibull distribution with shape parameter $k < 1$ (failure rate decreases over time). Note that this statement applies for disentrainment in space; the likelihood of a grain being deposited is thought to be Poissonian in time (i.e., constant disentrainment probability) (S. L. Fathel et al., 2015; Ancey et al., 2006), although the sub-critical grain travel time distributions discussed in Section 4.4 contradict this assertion. This mixed Weibull and exponential-like distribution is also supported by the analytical solution to the distribution of flight distances determined by Z. Wu et al. (2023). Similar to Section 4.4, we can again fit the Z. Wu et al. (2023) distribution to our PDFs of flight distances. Our PDFs of grain flight distance display heavier tails than predicted by the Z. Wu et al. (2023) distribution and are a better match to the Weibull distribution, although we note that the fit could be improved if $\langle u_g \rangle$ were not constrained to values close to the measured mean velocity (Figure 7c).

The two regimes proposed by Z. Wu et al. (2020) and recently supported by the numerical experiments of Yadav et al. (2026) suggests that grains traveling farther are more likely to experience the highest velocities and thus on average have a faster mean velocity over a flight (scaling $L_x \propto T_f$). The shorter trajectories, on the other hand, have on average a slower mean velocity (scaling $L_x \propto T_f^2$), with mean velocity proportional to flight time. The joint PDFs of grain travel time and flight distance (not shown), however, do not display this two-regime scaling based on our experimental results. Instead we find that the mean power law exponent fit to the joint PDF of T_f and L_x is 1.2 with a standard deviation of 0.16 across all experimental runs, which is a closer match to the scaling exponents measured by M. X. Liu et al. (2019). This range of observed scaling exponents also explicates the lack of agreement between our Weibull shape parameter (k = 0.40–0.73) and mean grain flight distances with the proposed theoretical shape ($k = 0.5$) and scale ($2\lambda = \langle L_x \rangle$) parameters of S. L. Fathel et al. (2015).

5 Discussion & Conclusions

Although the variable nature of bedload transport introduces many challenges when calculating sediment flux, the development of stochastic models has potential to improve sediment transport estimates over current deterministic frameworks. These stochastic models, however, require input in the form of probability distributions and statistical parameters for relevant bedload flight metrics—grain velocity, grain activity, flight travel distances and times. In this study, we analyzed a high-resolution dataset of grain trajectories collected at a range of flow conditions spanning the subcritical ($\tau_*/\tau_{*\,cr} = 0.78$) to supercritical ($\tau_*/\tau_{*\,cr} = 1.53$) sediment transport regimes. We implemented a hidden Markov model to segment grain trajectories into periods of motion and rest, which were then used to characterize the probability distributions of grain activity, velocity, acceleration, flight distance, and flight travel time across this range of transport conditions. Our primary conclusions are as follows:

1. **Implementation of a hidden Markov model for trajectory segmentation:** The use of a HMM to segment grain trajectories into periods of motion and rest offers numerous advantages over previous threshold-based methods. Since the HMM is trained on the full velocity distribution of grain motions, the classification is adaptive to local flow and transport conditions, rather than relying on a globally-defined velocity or displacement threshold. Further, the constant transition probabilities implicit to the HMM results in a temporal smoothing that allows the model to distinguish between velocity fluctuations (e.g., stationary grains jiggling in place or mobile grains experiencing momentary collisions) and genuine transitions between persistent downstream transport and sustained rest on the sediment bed.

   The selection of the HMM framework also has theoretical justification for use in a bedload transport context, as individual grain dynamics are frequently modeled as a Markov processes (Papanicolaou et al., 2002; Lisle et al., 1998). The constant transition probabilities, consistent with a telegraph process (Ancey et al., 2006), yield entrainment probabilities that agree with established empirical relationships (Figure 2).

2. **Validation of existing statistical frameworks:** Our results broadly validate statistical descriptions of bedload motion proposed by previous studies, particularly for flow conditions exceeding the critical Shields stress. The observed grain activity distributions are consistent with a negative binomial or Gamma distribution, as reported by Ancey et al. (2006) and González et al. (2017). The transition in distribution shape from exponential-like to Gaussian-like reflects the shift from highly intermittent, uncorrelated grain motions below and near onset to a greater quantity of moving grains influenced by collective entrainment effects at higher bed stresses. We confirm that streamwise and spanwise grain velocities exhibit an exponential distribution, consistent with prior observations and theory (S. L. Fathel et al., 2015; Furbish & Schmeeckle, 2013). Distributions of streamwise and spanwise particle accelerations display a Laplace distribution and are centered about zero, consistent with equilibrium transport conditions. For grain flight statistics, we observe that flight travel times are well-approximated by an exponential distribution for above-critical conditions, consistent with prior observations and the assumption of a fixed temporal disentrainment rate. Flight travel distances are well-described by the Weibull distributions in both the streamwise and spanwise directions, consistent with a decreasing spatial disentrainment rate.
3. **Emergence of anomalous dynamics below the onset of motion:** We identify unexpected behaviors in bedload statistics at and below the critical Shields stress, a regime that has received limited attention in previous experimental work despite its importance for understanding sediment transport in low-energy environments. We find that well-accepted probability distributions for bedload motion parameters, identified above, fit progressively more poorly as flow conditions approach and fall below the threshold of motion. Notably, streamwise grain velocities for sub-critical to critical conditions exhibit distributions that are more peaked than an exponential and have heavier tails (Figure 4a), contrary to the light-tailed expectation for small particle numbers (Furbish & Schmeeckle, 2013). Similarly, the exponential distribution for flight travel time becomes increasingly peaked with heavier tails at sub-critical conditions (Figure 6b). This deviation suggests that the assumption of a constant temporal disentrainment probability breaks down in this highly intermittent regime. Broadly, this behavior may indicate that near-threshold grain motion involves a mixture of mostly short, slow displacements (e.g., grains rolling out of pockets) and intermittent longer flights as occasional energetic turbulent structures entrain small numbers of sand grains. The breakdown of exponential travel time distributions and the emergence of heavier-tailed flight distance distributions below threshold indicate that the local diffusion regime may transition from normal to anomalous in this highly intermittent transport state.

   We also examine the analytical solutions for bedload flight statistics proposed by Z. Wu et al. (2023) and observe that their distribution for flight travel times is a better fit to our grain flight data than the exponential distribution, at least at and below the threshold of motion. However, their flight distance distribution appears to fit more poorly than the Weibull distribution. In addition to providing a better fit for sub-threshold grain flight statistics, we note that analytical solutions may also yield useful physical parameters (grain velocity, disentrainment rate) that can inform us about system dynamics.
4. **Asymmetry in grain acceleration distributions:** While ensemble-averaged streamwise and spanwise grain accelerations remain close to zero for all flow conditions, supporting the quasi-equilibrium transport assumption implicit in many bedload models, we calculate skewness and identify an asymmetry in the distribution of streamwise grain accelerations (Figure 5c). At sub-critical conditions, acceleration PDFs exhibit negative skewness, hypothesized to be evidence of "flight-crash" dynamics where grains experience a relatively gentle acceleration followed

by rapid deceleration upon colliding with the bed. This behavior resembles flight-crash events observed in turbulent flows and is associated with intermittency in turbulent systems (Xu et al., 2014; Švančara & La Mantia, 2019). Above the critical Shields stress, the skewness becomes positive, suggesting a reversal of dynamics to a "lift and settle" behavior, with rapid accelerations as grains are lifted off the bed (possibly by turbulent sweeps and ejection events) followed by gentler deceleration as grains settle through regions of lower-velocity fluid. This transition in acceleration asymmetry may reflect a fundamental change in the dominant entrainment and disentrainment mechanisms across the threshold of motion. The varying skewness suggests that higher-order moments of the acceleration distribution may carry important information about transport regime transitions.

Our results provide an extensive dataset that can be used for validating numerical simulations and analytical solutions for stochastic sediment transport models, particularly at conditions below the onset of motion. The systematic characterization of bedload motion probability distributions at a range of Shields stresses from below to exceeding the critical Shields stress enables improved parameterization of both activity-based and entrainment-based formulations of sediment flux.

Open Research Section

All relevant data and code used to generate the figures in this paper are deposited in Figshare, a free and open repository. These data sets can be accessed using the following link: https://figshare.com/s/ec90be61ecd62ec3d049 (Bodek, Wang, Shattuck, O'Hern, & Ouellette, 2026).

Acknowledgments

Financial support was provided by the Army Research Office (ARO Award #W911NF-23-1-0032). The authors thank Stanford Research Computing for computational support through the Sherlock cluster and Patrick Nicholson for assistance with HMM implementation. The authors declare no conflicts of interest relevant to this study.

References

Ancey, C. (2010). Stochastic modeling in sediment dynamics: Exner equation for planar bed incipient bed load transport conditions. *Journal of Geophysical Research: Earth Surface*, *115*(F2).

Ancey, C., Böhm, T., Jodeau, M., & Frey, P. (2006, July). Statistical description of sediment transport experiments. *Phys. Rev. E*, *74*(1), 011302. doi: 10.1103/PhysRevE.74.011302

Ancey, C., Davison, A., Böhm, T., Jodeau, M., & Frey, P. (2008). Entrainment and motion of coarse particles in a shallow water stream down a steep slope. *Journal of Fluid Mechanics*, *595*, 83–114.

Ancey, C., & Heyman, J. (2014). A microstructural approach to bed load transport: mean behaviour and fluctuations of particle transport rates. *Journal of Fluid Mechanics*, *744*, 129–168.

Baum, L. E. (1972). An inequality and associated maximization technique in statistical estimation for probabilistic functions of markov processes. *Inequalities*, *3*(1), 1–8.

Baum, L. E., & Eagon, J. A. (1967). An inequality with applications to statistical estimation for probabilistic functions of markov processes and to a model for ecology. *Bulletin of the American Mathematical Society*, *73*(3), 360–363.

Baum, L. E., & Petrie, T. (1966). Statistical inference for probabilistic functions of finite state markov chains. *The annals of mathematical statistics*, *37*(6), 1554–

1563.

Benavides, S. J., Deal, E., Rushlow, M., Venditti, J. G., Zhang, Q., Kamrin, K., & Perron, J. T. (2022). The impact of intermittency on bed load sediment transport. *Geophysical Research Letters*, *49*(5), e2021GL096088.

Benavides, S. J., Deal, E., Venditti, J. G., Bradley, R., Zhang, Q., Kamrin, K., & Perron, J. T. (2023). How fast or how many? sources of intermittent sediment transport. *Geophysical Research Letters*, *50*(9), e2022GL101919.

Bhattacharya, B., Price, R., & Solomatine, D. (2005). Data-driven modelling in the context of sediment transport. *Physics and Chemistry of the Earth, Parts A/B/C*, *30*(4-5), 297–302.

Bodek, S., Wang, D., Shattuck, M. D., O'Hern, C. S., & Ouellette, N. T. (2026). Ensemble statistics of bedload transport: Dataset of grain motion and rest measurements. *figshare [dataset]*. doi: https://figshare.com/s/ec90be61ecd62ec3d049

Bodek, S., Wang, D., Shattuck, M. D., O'Hern, C. S., & Ouellette, N. T. (2026a). Anisotropic stress history effects in erodible sediment beds. *Journal of Geophysical Research: Earth Surface*, *131*(1), e2025JF008561.

Bodek, S., Wang, D., Shattuck, M. D., O'Hern, C. S., & Ouellette, N. T. (2026b). Ensemble statistics of bedload transport. Part 2: Stress history effects [manuscript submitted for publication].

Bohorquez, P., & Ancey, C. (2015). Stochastic-deterministic modeling of bed load transport in shallow water flow over erodible slope: Linear stability analysis and numerical simulation. *Advances in water resources*, *83*, 36–54.

Bradley, D. N., Tucker, G. E., & Benson, D. A. (2010). Fractional dispersion in a sand bed river. *Journal of Geophysical Research: Earth Surface*, *115*(F1).

Campagnol, J., Radice, A., Ballio, F., & Nikora, V. (2015). Particle motion and diffusion at weak bed load: accounting for unsteadiness effects of entrainment and disentrainment. *Journal of Hydraulic Research*, *53*(5), 633–648.

Campagnol, J., Radice, A., Nokes, R., Bulankina, V., Lescova, A., & Ballio, F. (2013). Lagrangian analysis of bed-load sediment motion: database contribution. *Journal of Hydraulic Research*, *51*(5), 589–596.

Cecchetto, M., Tregnaghi, M., Bottacin-Busolin, A., Tait, S., Cotterle, L., & Marion, A. (2018). Diffusive regimes of the motion of bed load particles in open channel flows at low transport stages. *Water Resources Research*, *54*(11), 8674–8691.

Cheng, N.-S., & Chiew, Y.-M. (1998). Pickup probability for sediment entrainment. *Journal of Hydraulic Engineering*, *124*(2), 232–235.

Cournapeau, D., Pedregosa, F., Varoquaux, G., Lebedev, S., Lee, A., Danielson, M., et al. (2024). *hmmlearn.* GitHub. Retrieved from `https://github.com/hmmlearn/hmmlearn` (Software Version 0.3.3)

Dey, S., & Ali, S. Z. (2019). Bed sediment entrainment by streamflow: State of the science. *Sedimentology*, *66*(5), 1449–1485.

Durán, O., Andreotti, B., & Claudin, P. (2012). Numerical simulation of turbulent sediment transport, from bed load to saltation. *Physics of Fluids*, *24*(10).

Eddy, S. R. (1996). Hidden markov models. *Current opinion in structural biology*, *6*(3), 361–365.

Einstein, H. A. (1937). *Bed load transport as a probability problem* (PhD Thesis). ETH Zurich, Zurich Switzerland. (English translation by W.W. Sayre, in *Sedimentation: Symposium to Honor Professor H. A. Einstein*, Appendix C, edited by H.-W. Shen, pp. C1–C105, Colorado State University, Fort Collins, CO., 1972)

Einstein, H. A. (1942). Formulas for the transportation of bed load. *Transactions of the American Society of civil Engineers*, *107*(1), 561–577.

Einstein, H. A. (1950). *The bed-load function for sediment transportation in open channel flows* (Vol. 1026). US Government Printing Office.

Einstein, H. A., & El-Samni, E.-S. A. (1949, July). Hydrodynamic Forces on a Rough Wall. *Rev. Mod. Phys.*, *21*(3), 520–524. doi: 10.1103/RevModPhys.21.520

Ephraim, Y., & Merhav, N. (2002). Hidden markov processes. *IEEE Transactions on information theory*, *48*(6), 1518–1569.

Escauriaza, C., González, C., Williams, M. E., & Brevis, W. (2023, March). Models of bed-load transport across scales: turbulence signature from grain motion to sediment flux. *Stochastic Environ. Res. Risk Assess.*, *37*(3), 1039–1052. doi: 10.1007/s00477-022-02333-9

Fan, N., Singh, A., Guala, M., Foufoula-Georgiou, E., & Wu, B. (2016). Exploring a semimechanistic episodic langevin model for bed load transport: Emergence of normal and anomalous advection and diffusion regimes. *Water Resources Research*, *52*(4), 2789–2801.

Fan, N., Zhong, D., Wu, B., Foufoula-Georgiou, E., & Guala, M. (2014). A mechanistic-stochastic formulation of bed load particle motions: From individual particle forces to the fokker-planck equation under low transport rates. *Journal of Geophysical Research: Earth Surface*, *119*(3), 464–482.

Fathel, S., Furbish, D., & Schmeeckle, M. (2016). Parsing anomalous versus normal diffusive behavior of bedload sediment particles. *Earth Surface Processes and Landforms*, *41*(12), 1797–1803.

Fathel, S. L., Furbish, D. J., & Schmeeckle, M. W. (2015). Experimental evidence of statistical ensemble behavior in bed load sediment transport. *Journal of Geophysical Research: Earth Surface*, *120*(11), 2298–2317.

Foufoula-Georgiou, E., & Stark, C. (2010). Introduction to special section on stochastic transport and emergent scaling on earth's surface: Rethinking geomorphic transport—stochastic theories, broad scales of motion and nonlocality. *Journal of Geophysical Research: Earth Surface*, *115*(F2).

Fredsoe, J., & Deigaard, R. (1992). *Mechanics of coastal sediment transport* (Vol. 3). World scientific publishing company.

Furbish, D. J. (2025). *Statistical Physics of Rarefied Sediment Particle Motions and Transport Applications to Hillslopes and Rivers.* ebook. Retrieved from `https://cdn.vanderbilt.edu/t2-my/my-prd/wp-content/uploads/sites/978/2025/08/Preview.pdf`

Furbish, D. J., Fathel, S. L., Schmeeckle, M. W., Jerolmack, D. J., & Schumer, R. (2017). The elements and richness of particle diffusion during sediment transport at small timescales. *Earth Surface Processes and Landforms*, *42*(1), 214–237.

Furbish, D. J., Haff, P. K., Roseberry, J. C., & Schmeeckle, M. W. (2012, September). A probabilistic description of the bed load sediment flux: 1. Theory. *J. Geophys. Res. Earth Surf.*, *117*(F3). doi: 10.1029/2012JF002352

Furbish, D. J., Roseberry, J. C., & Schmeeckle, M. W. (2012). A probabilistic description of the bed load sediment flux: 3. the particle velocity distribution and the diffusive flux. *Journal of Geophysical Research: Earth Surface*, *117*(F3).

Furbish, D. J., & Schmeeckle, M. W. (2013, March). A probabilistic derivation of the exponential-like distribution of bed load particle velocities. *Water Resour. Res.*, *49*(3), 1537–1551. doi: 10.1002/wrcr.20074

Furbish, D. J., Schmeeckle, M. W., Schumer, R., & Fathel, S. L. (2016). Probability distributions of bed load particle velocities, accelerations, hop distances, and travel times informed by jaynes's principle of maximum entropy. *Journal of Geophysical Research: Earth Surface*, *121*(7), 1373–1390.

Galanis, M., Shattuck, M. D., O'Hern, C. S., & Ouellette, N. T. (2022, January). Directional strengthening and weakening in hydrodynamically sheared granular beds. *Phys. Rev. Fluids*, *7*(1), 013802. doi: 10.1103/PhysRevFluids.7.013802

Ganti, V., Meerschaert, M. M., Foufoula-Georgiou, E., Viparelli, E., & Parker, G. (2010). Normal and anomalous diffusion of gravel tracer particles in rivers.

Journal of Geophysical Research: Earth Surface, *115*(F2).
García, M. H. (2013, May). Sediment Transport and Morphodynamics. *Sedimentation Engineering*, 21–163. doi: 10.1061/9780784408148.ch02
Gibbs, J. W. (1902). *Elementary principles in statistical mechanics: developed with especial reference to the rational foundations of thermodynamics*. C. Scribner's sons.
González, C., Richter, D. H., Bolster, D., Bateman, S., Calantoni, J., & Escauriaza, C. (2017, February). Characterization of bedload intermittency near the threshold of motion using a Lagrangian sediment transport model. *Environ. Fluid Mech.*, *17*(1), 111–137. doi: 10.1007/s10652-016-9476-x
Guy, H. P., Simons, D. B., & Richardson, E. V. (1966). *Summary of alluvial channel data from flume experiments, 1956-61.* US Government Printing Office.
Hamilton, J. D. (1989). A new approach to the economic analysis of nonstationary time series and the business cycle. *Econometrica: Journal of the econometric society*, 357–384.
Helbing, D. (2001). Traffic and related self-driven many-particle systems. *Reviews of modern physics*, *73*(4), 1067.
Heyman, J., Bohorquez, P., & Ancey, C. (2016). Entrainment, motion, and deposition of coarse particles transported by water over a sloping mobile bed. *Journal of Geophysical Research: Earth Surface*, *121*(10), 1931–1952.
Heyman, J., Ma, H., Mettra, F., & Ancey, C. (2014). Spatial correlations in bed load transport: Evidence, importance, and modeling. *Journal of Geophysical Research: Earth Surface*, *119*(8), 1751–1767.
Jain, S. C. (1992). Note on lag in bedload discharge. *Journal of Hydraulic Engineering*, *118*(6), 904–917.
Jensen, M. H., Johansen, A., & Simonsen, I. (2003). Inverse statistics in economics: the gain–loss asymmetry. *Physica A: Statistical Mechanics and its Applications*, *324*(1-2), 338–343.
Kalinske, A. (1947). Movement of sediment as bed load in rivers. *Eos, Transactions American Geophysical Union*, *28*(4), 615–620.
Kirchner, J. W., Dietrich, W. E., Iseya, F., & Ikeda, H. (1990, August). The variability of critical shear stress, friction angle, and grain protrusion in water-worked sediments. *Sedimentology*, *37*(4), 647–672. doi: 10.1111/j.1365-3091.1990.tb00627.x
Krogh, A., Brown, M., Mian, I. S., Sjölander, K., & Haussler, D. (1994). Hidden markov models in computational biology: Applications to protein modeling. *Journal of molecular biology*, *235*(5), 1501–1531.
Lajeunesse, E., Malverti, L., & Charru, F. (2010, December). Bed load transport in turbulent flow at the grain scale: Experiments and modeling. *J. Geophys. Res. Earth Surf.*, *115*(F4). doi: 10.1029/2009JF001628
Lelouvetel, J., Bigillon, F., Doppler, D., Vinkovic, I., & Champagne, J.-Y. (2009). Experimental investigation of ejections and sweeps involved in particle suspension. *Water resources research*, *45*(2).
Li, D., Sun, Y., Sun, J., Wang, X., & Zhang, X. (2022). An advanced approach for the precise prediction of water quality using a discrete hidden markov model. *Journal of Hydrology*, *609*, 127659.
Lisle, I., Rose, C., Hogarth, W., Hairsine, P., Sander, G., & Parlange, J.-Y. (1998). Stochastic sediment transport in soil erosion. *Journal of Hydrology*, *204*(1-4), 217–230.
Liu, C., Zhang, L., Zhang, Y., Jiang, X., Liu, F., Gu, L., & Lu, J. (2024). Study on the motion characteristics of bedload sediment particles under different sediment transport intensities. *River*, *3*(2), 140–151.
Liu, M. X., Pelosi, A., & Guala, M. (2019, November). A Statistical Description of Particle Motion and Rest Regimes in Open-Channel Flows Under Low Bedload Transport. *J. Geophys. Res. Earth Surf.*, *124*(11), 2666–2688. doi:

10.1029/2019JF005140
Luque, F., & Erosion, R. (1974). *Transport of bed-load sediment* (Unpublished doctoral dissertation). Delft Technical University Delft, The Netherlands.
Markov, A. A. (1913). An example of statistical investigation of the text Eugene Onegin concerning the connection of samples in chains [in Russian]. *Bulletin of the Imperial Academy of Sciences of St. Petersburg*, *7*(3), 153–162. (English translation by Alexander Y. Nitussov, Lioudmila Voropai, Gloria Custance and David Link (2006). Science in Context, 19(4), 591—600.)
Martin, R. L., Jerolmack, D. J., & Schumer, R. (2012). The physical basis for anomalous diffusion in bed load transport. *Journal of Geophysical Research: Earth Surface*, *117*(F1).
Mordant, N., Crawford, A. M., & Bodenschatz, E. (2004, June). Experimental Lagrangian acceleration probability density function measurement. *Physica D*, *193*(1), 245–251. doi: 10.1016/j.physd.2004.01.041
Nikora, V., Habersack, H., Huber, T., & McEwan, I. (2002). On bed particle diffusion in gravel bed flows under weak bed load transport. *Water Resources Research*, *38*(6), 17–1.
Niño, Y., & García, M. (1998). Using lagrangian particle saltation observations for bedload sediment transport modelling. *Hydrological Processes*, *12*(8), 1197–1218.
O'Riordan, C. A., Monismith, S. G., & Koseff, J. R. (1993, December). A study of concentration boundary-layer formation over a bed of model bivalves. *Limnol. Oceanogr.*, *38*(8), 1712–1729. doi: 10.4319/lo.1993.38.8.1712
Ouellette, N. T., Xu, H., & Bodenschatz, E. (2006, February). A quantitative study of three-dimensional Lagrangian particle tracking algorithms. *Exp. Fluids*, *40*(2), 301–313. doi: 10.1007/s00348-005-0068-7
Papanicolaou, A., Diplas, P., Evaggelopoulos, N., & Fotopoulos, S. (2002). Stochastic incipient motion criterion for spheres under various bed packing conditions. *Journal of Hydraulic Engineering*, *128*(4), 369–380.
Pelosi, A., Parker, G., Schumer, R., & Ma, H.-B. (2014). Exner-based master equation for transport and dispersion of river pebble tracers: Derivation, asymptotic forms, and quantification of nonlocal vertical dispersion. *Journal of Geophysical Research: Earth Surface*, *119*(9), 1818–1832.
Rabiner, L. R. (1989). A tutorial on hidden markov models and selected applications in speech recognition. *Proceedings of the IEEE*, *77*(2), 257–286.
Radice, A., Sarkar, S., & Ballio, F. (2017, July). Image-based Lagrangian Particle Tracking in Bed-load Experiments. *Journal of Visualized Experiments : JoVE*(125), 55874. doi: 10.3791/55874
Rebai, D., Radice, A., & Ballio, F. (2024, August). Traveling or Jiggling: Particle Motion Modes and Their Relative Contribution to Bed-Load Variables. *J. Geophys. Res. Earth Surf.*, *129*(8), e2024JF007637. doi: 10.1029/2024JF007637
Roseberry, J. C., Schmeeckle, M. W., & Furbish, D. J. (2012, September). A probabilistic description of the bed load sediment flux: 2. Particle activity and motions. *J. Geophys. Res. Earth Surf.*, *117*(F3). doi: 10.1029/2012JF002353
Salevan, J. C., Clark, A. H., Shattuck, M. D., O'Hern, C. S., & Ouellette, N. T. (2017, November). Determining the onset of hydrodynamic erosion in turbulent flow. *Phys. Rev. Fluids*, *2*(11), 114302. doi: 10.1103/PhysRevFluids.2.114302
Schmeeckle, M. W. (2014). Numerical simulation of turbulence and sediment transport of medium sand. *Journal of Geophysical Research: Earth Surface*, *119*(6), 1240–1262.
Schmeeckle, M. W., & Nelson, J. M. (2003, April). Direct numerical simulation of bedload transport using a local, dynamic boundary condition. *Sedimentology*, *50*(2), 279–301. doi: 10.1046/j.1365-3091.2003.00555.x

Schumer, R., Meerschaert, M. M., & Baeumer, B. (2009). Fractional advection-dispersion equations for modeling transport at the earth surface. *Journal of Geophysical Research: Earth Surface*, *114*(F4).

Shim, J., & Duan, J. (2019). Experimental and theoretical study of bed load particle velocity. *Journal of Hydraulic Research*, *57*(1), 62–74.

Shim, J., & Duan, J. G. (2017, March). Experimental study of bed-load transport using particle motion tracking. *Int. J. Sediment Res.*, *32*(1), 73–81. doi: 10.1016/j.ijsrc.2016.10.002

Sun, Z., & Donahue, J. (2000). Statistically derived bedload formula for any fraction of nonuniform sediment. *Journal of Hydraulic Engineering*, *126*(2), 105–111.

Švančara, P., & La Mantia, M. (2019). Flight-crash events in superfluid turbulence. *Journal of Fluid Mechanics*, *876*, R2.

Thyer, M., & Kuczera, G. (2003). A hidden markov model for modelling long-term persistence in multi-site rainfall time series 1. model calibration using a bayesian approach. *Journal of Hydrology*, *275*(1-2), 12–26.

Vanoni, V. A. (2006, March). Sediment Transportation Mechanics. *Sedimentation Engineering*, 11–189. doi: 10.1061/9780784408230.ch02

Viterbi, A. (1967). Error bounds for convolutional codes and an asymptotically optimum decoding algorithm. *IEEE transactions on Information Theory*, *13*(2), 260–269.

Weeks, E. R., Urbach, J., & Swinney, H. L. (1996). Anomalous diffusion in asymmetric random walks with a quasi-geostrophic flow example. *Physica D: Nonlinear Phenomena*, *97*(1-3), 291–310.

Wu, F.-C., & Chou, Y.-J. (2003). Rolling and lifting probabilities for sediment entrainment. *Journal of Hydraulic Engineering*, *129*(2), 110–119.

Wu, F.-C., & Lin, Y.-C. (2002). Pickup probability of sediment under log-normal velocity distribution. *Journal of Hydraulic Engineering*, *128*(4), 438–442.

Wu, F.-C., & Yang, K.-H. (2004). A stochastic partial transport model for mixed-size sediment: Application to assessment of fractional mobility. *Water resources research*, *40*(4).

Wu, Z., Furbish, D., & Foufoula-Georgiou, E. (2020). Generalization of hop distance-time scaling and particle velocity distributions via a two-regime formalism of bedload particle motions. *Water Resources Research*, *56*(1), e2019WR025116.

Wu, Z., Jiang, W., Zeng, L., & Fu, X. (2023). Theoretical analysis for bedload particle deposition and hop statistics. *Journal of Fluid Mechanics*, *954*, A11.

Wu, Z., Singh, A., Foufoula-Georgiou, E., Guala, M., Fu, X., & Wang, G. (2021). A velocity-variation-based formulation for bedload particle hops in rivers. *Journal of Fluid Mechanics*, *912*, A33.

Xu, H., Pumir, A., Falkovich, G., Bodenschatz, E., Shats, M., Xia, H., ... Boffetta, G. (2014). Flight–crash events in turbulence. *Proceedings of the National Academy of Sciences*, *111*(21), 7558–7563.

Yadav, A., Cúñez, F. D., & Glade, R. C. (2026). Flow strength and methodological controls on statistical ensemble behavior of bedload kinematics. *ESS Open Archive*. doi: 10.22541/essoar.15004695/v1